INTERNATIONAL JOURNAL FOR NUMERICAL METHODS IN FLUIDS
Int. J. Numer. Meth. Fluids 2000; **32**: 79–96

A boundary element method and spectral analysis model for small-amplitude viscous fluid sloshing in couple with structural vibrations

Yuelong Zang[a,*], Songtao Xue[b] and Satoshi Kurita[c]

[a] *Mechanical Engineering Department, Fuzhou University, Fuzhou 350002, China*
[b] *Engineering Mechanics Department, Tongji University, Shanghai 200092, China*
[c] *Department of Architecture, Faculty of Engineering, Tohoko University, Sedai, Japan*

SUMMARY

A boundary element method (BEM) is presented for the coupled motion analysis of structural vibrations with small-amplitude fluid sloshing in two-dimensional space. The linearized *Navier–Stokes* equations are considered in the frequency domain and transformed into a *Laplace* equation and a *Helmholtz* equation with pure imaginary constant. An appropriate fundamental solution for the *Helmholtz* equation is provided. The conditions of zero stress are imposed on the free surface, and non-slip conditions of fluid particles are imposed on the walls of the container. For rigid motion models, the expressions for added mass and added damping to the structural motion equations are obtained. Numerical examples are presented. Copyright © 2000 John Wiley & Sons, Ltd.

KEY WORDS: BEM; fluid sloshing; structural vibrations; tuned liquid damper

1. INTRODUCTION

Every fluid has a certain viscosity, primarily dependent on the temperature. The effect of viscosity is most significant near rigid walls or, for fluid sloshing, at/or near a resonant frequency. The linear potential theory cannot account for the viscous effect, and when the fluid is excited near its resonant frequency, the motion analysis by the linear potential theory gives unpractical results. If a fluid has no viscosity, its sloshing will only absorb energy, but cannot dissipate energy. For the purpose of analysing fluid sloshing in a tuned liquid damper (TLD), viscosity must be considered in the analysis. Since a TLD usually contains shallow water, the interface between the water and the container walls takes a large proportion. Besides, a TLD is usually designed to work at or near its resonant frequency to maximize the absorbed and dissipated energy from the structure on which the TLD is installed.

* Correspondence to: Mechanics Division, Mechanical Engineering Department, Fuzhou University, Fuzhou, Fujian Province, 350002, China.

CCC 0271–2091/2000/010079–18$17.50

Received March 1998
Revised November 1998

Problems of fluid sloshing have been studied by many people, both in finite element methods (FEM) and boundary element methods (BEM). Ikegawa [1] analyzed the non-linear sloshing of a fluid in a two-dimensional rectangular container subjected to horizontal excitation. Extending Ikegawa's method, Washizu *et al.* [2] analyzed the non-linear sloshing of a fluid in a container subjected to vertical excitation, and Nakayama *et al.* [3] analyzed the sloshing problem of fluid in a rectangular container subjected to pitching excitation using the FEM. In particular, Lepelletier *et al.* [4] used the FEM to solve the non-linear fluid oscillations in a rectangular tank using a non-linear, dispersive and dissipative model. Nakayama [5,6] also used the BEM to solve the same problem. Sugino and Tosaka [7] proposed a BEM solution procedure based on the mixed *Eulerian–Lagrangian* approach to solve the non-linear fluid sloshing problem. Shinkai [8,9] analyzed the three-dimensional sloshing problem using the BEM together with the perturbation method. Ohyama and Fujii [10] carried out numerical simulations for a circular TLD by using the BEM. All the above-mentioned BEMs for fluid sloshing used the assumption of inviscid and incompressible fluid, and thus the control equation became the well-known *Laplace* equation. The difficulty was only the non-linearity of the free surface condition, which may be treated rather easily by the time-dependent BEM [5].

Sun, Fujino, Pacheco and co-workers [11–15] proposed a potential theory based on the shallow water theory in combination with the boundary layer theory, i.e. the fluid viscosity is considered only in the boundary layer. Modi and Welt [16] carried out an experimental and analytical study on a nutational damper (annular tanker). Their theoretical investigation was concerned with the energy dissipation mechanism assuming a potential flow with a non-linear free surface condition in conjunction with the boundary layer correction. Procedures including free surface non-linearities and fluid viscosity make up the main part of the energy dissipation and generally give better results for free surface wave forms than linear theories.

Most of the research work carried out for fluid sloshing used the potential theory in the time domain. This requires that the container's motions be known prior to the solution of the fluid sloshing. This is impossible for the coupled motion analysis of a TLD installed on a structure, where the motions of the structure and of the fluid are interdependent. By assuming that the response of a structure with a TLD can be considered as the summation of the responses to excitations of all frequencies, the problem is reduced to the analysis of the fluid sloshing excited by the container's unit amplitude monochromatic motions in its known motion models. This application of spectral analysis is not novel in engineering, and it is valid provided the fluid wave amplitude does not make the non-linear phenomena on the free surface become dominant.

The present work is based on the spectral analysis method to study the fluid sloshing coupled with the structural motions. The analysis model is based on the linearized *Navier–Stokes* equations in two-dimensional form, considering the viscosity within the whole fluid domain. This is an improvement over the potential theory. Moreover, the present model gives the BEM for the *Helmholtz* equation with pure imaginary constant.

For different frequencies, the effect of sloshing of the fluid on a structure is the forces and moments acting on the structure, and they are dependent on the container's motion amplitudes so that they are further expressed as the added mass and added damping to the structure. In this paper, the expressions of the added mass and damping are given. The added mass and added damping are dependent on the frequency. The motion analysis of the structure may be

directly carried out by adding the added mass and damping matrices to the 'dry' structure, i.e. the structure without fluid in the container.

2. MATHEMATICAL FORMULATIONS

Linearized *Navier–Stokes* equations in two-dimensional form for Newtonian fluids are [17]

$$\frac{\partial U}{\partial t} = -\frac{1}{\rho}\frac{\partial P}{\partial x} + v\left(\frac{\partial^2 U}{\partial x^2} + \frac{\partial^2 U}{\partial y^2}\right), \quad \text{in } \Omega, \tag{1}$$

$$\frac{\partial V}{\partial t} = -\frac{1}{\rho}\frac{\partial P}{\partial y} - g + v\left(\frac{\partial^2 V}{\partial x^2} + \frac{\partial^2 V}{\partial y^2}\right), \quad \text{in } \Omega, \tag{2}$$

where U and V are the fluid velocity components in the x- and y-directions respectively, P is the mean pressure, ρ is the fluid density, v is the fluid kinematic viscosity, g is the gravitational acceleration and Ω denotes the fluid domain. The co-ordinate system Oxy is shown in Figure 1. For an incompressible fluid, the fluid motion also satisfies the following continuity equation:

$$\frac{\partial U}{\partial x} + \frac{\partial V}{\partial y} = 0, \quad \text{in } \Omega. \tag{3}$$

For steady state sinusoidal motions, the velocity components and the mean pressure may be written as

$$U = u\, \mathrm{e}^{-\mathrm{i}\omega t}, \tag{4}$$

$$V = v\, \mathrm{e}^{-\mathrm{i}\omega t}, \tag{5}$$

$$P = p\, \mathrm{e}^{-\mathrm{i}\omega t} - \rho g y, \tag{6}$$

where ω is the angular frequency. By Lamb's transform [17],

$$u = \frac{\partial \phi}{\partial x} - \frac{\partial \psi}{\partial y}, \tag{7}$$

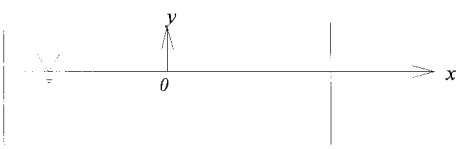

Figure 1. The co-ordinate system of the problem.

$$v = \frac{\partial \phi}{\partial y} + \frac{\partial \psi}{\partial x}, \tag{8}$$

$$p = \mathrm{i}\omega\rho\phi. \tag{9}$$

The control equations (1)–(3) and the corresponding boundary conditions may be written as

$$\nabla^2 \phi = 0 \quad \text{in } \Omega, \tag{10}$$

$$\nabla^2 \psi + \frac{\mathrm{i}\omega}{v}\psi = 0 \quad \text{in } \Omega, \tag{11}$$

$$\frac{\partial}{\partial s}\left(\frac{\partial \psi}{\partial n}\right) + \frac{1}{\rho_0}\frac{\partial \phi}{\partial n} - \frac{1}{\rho_0}\frac{\partial \psi}{\partial s} + \frac{\partial^2 \phi}{\partial s^2} + \frac{\mathrm{i}\omega}{2v}\phi = 0 \quad \text{on } S_1, \tag{12}$$

$$\frac{\partial}{\partial s}\left(\frac{\partial \phi}{\partial n}\right) - \frac{1}{\rho_0}\frac{\partial \psi}{\partial n} - \frac{1}{\rho_0}\frac{\partial \phi}{\partial s} - \frac{\partial^2 \psi}{\partial s^2} - \frac{\mathrm{i}\omega}{2v}\psi = 0 \quad \text{on } S_1, \tag{13}$$

$$\frac{\partial \phi}{\partial n} - \frac{\partial \psi}{\partial s} = u_0 n_1 + v_0 n_2 \quad \text{on } S_2, \tag{14}$$

$$\frac{\partial \psi}{\partial n} + \frac{\partial \phi}{\partial s} = -u_0 n_2 + v_0 n_1 \quad \text{on } S_2, \tag{15}$$

where ρ_0 is the radius of the boundary line, u_0 and v_0 are the wall's moving velocity components at the point of contact with the fluid particle, $\partial/\partial n$ denotes the normal derivative, $\partial/\partial s$ denotes the derivative along the boundary line, S_1 is the free surface and S_2 is the interface of the fluid and the container's wall.

3. BOUNDARY INTEGRAL EQUATIONS OF THE PROBLEM

By Green's identity, it is easy to transform Equation (10) into the boundary integral equation as

$$\alpha(q)\phi(q) + \int_S \left[\frac{\partial G_1(p, q)}{\partial n_p}\phi(p) - G_1(p, q)\frac{\partial \phi(p)}{\partial n_p}\right] \mathrm{d}S_p = 0, \tag{16}$$

where $G_1(p, q)$ is the fundamental solution to the Laplace equation,

$$G_1(p, q) = \ln\frac{1}{r}, \quad r = |\mathbf{r}_p - \mathbf{r}_q|, \tag{17}$$

where $\mathbf{r}_p$, $\mathbf{r}_q$ are the position vectors of the field point and the source point respectively, and $\alpha(q)$ is

$$\alpha(q) = \begin{cases} 2\pi & q \in \Omega \\ \pi & q \in S. \\ 0 & q \notin \Omega \end{cases}$$

To transform Equation (11) into a boundary integral equation, an appropriate fundamental solution must first be solved for. Considering the polar symmetry, we may rewrite Equation (11) as

$$\frac{\mathrm{d}^2 G_2}{\mathrm{d}r^2} + \frac{1}{r}\frac{\mathrm{d}G_2}{\mathrm{d}r} + \frac{\mathrm{i}\omega}{v} G_2 = 0, \tag{18}$$

where the fundamental solution, G_2, is in substitution of ψ. Equation (18) is a homogeneous differential equation, and a non-trivial solution is solved for. Letting

$$Z = \sqrt{-\frac{\mathrm{i}\omega}{v}}\, r,$$

we have

$$\frac{\mathrm{d}G_2}{\mathrm{d}z^2} + \frac{1}{z}\frac{\mathrm{d}G_2}{\mathrm{d}z} - G_2 = 0. \tag{19}$$

Equation (19) is the well-known differential equation related to *Bessel* functions of zeroth order. *Bessel* functions have many different types [20], such as $J_0(z)$, $Y_0(z)$, $H_0(z)$, $K_0(z)$, $I_0(z)$, etc. The linear combinations of these zeroth order *Bessel* functions also satisfy Equation (19).

As a two-dimensional fundamental solution, it must be convergent when the field point is far away from the source point. This seems to be prerequisite to fundamental solutions in BEMs. When the field point is far away from the source point and the value of the fundamental solution becomes larger, i.e. the fundamental solution is divergent, the portion of the boundary that is far away from the source point will have a larger influence on the source point. This is in conflict to the practical situation. Usually, the closer the portion of the boundary is to the source point, the more it will influence the behavior of the source point.

Besides, in the two-dimensional case, the type of singularity of the fundamental solutions is logarithmic, and the singularity of the first-order derivative of the fundamental solutions is of one order, i.e. of the type $1/r$, where r is the distance between the source point and the field point. Hypersingularity also occurs in some special problems, but usually it is avoided.

Among the zeroth order *Bessel* functions, $J_0(z)$, $Y_0(z)$, $H_0(z)$, $K_0(z)$, $I_0(z)$, and their linear combinations, the solution that satisfies the above two conditions is to be determined. After investigation of the asymptotic behavior as z approaches infinity, $K_0(z)$ is chosen as the fundamental solution that converges to zero quickly as r approaches infinity, if z is taken as

$$z = \sqrt{-\frac{\mathrm{i}\omega}{\nu}}\, r = \sqrt{\frac{\omega}{\nu}}\left(\frac{\sqrt{2}}{2} - \mathrm{i}\,\frac{\sqrt{2}}{2}\right) r.$$

Other forms of the *Bessel* functions do not satisfy the convergence condition when r approaches infinity.

The normal derivative of $G_2(p, q)$ is

$$\frac{\partial G_2}{\partial n} = -\sqrt{\frac{\omega}{\nu}}\left(\frac{\sqrt{2}}{2} - \mathrm{i}\,\frac{\sqrt{2}}{2}\right) K_1(z)\,\frac{\partial r}{\partial n}.$$

The boundary integral equation for Equation (11) can be written as

$$\alpha(q)\psi(q) + \int_S \left[\frac{\partial G_2(p, q)}{\partial n_p}\,\psi(p) - G_2(p, q)\,\frac{\partial \psi(p)}{\partial n_p}\right] \mathrm{d}S_p = 0. \tag{20}$$

A numerical test is carried out to test the fundamental solution G_2 with Equation (20) for the *Bessel* function $\psi(x, y) = J_0(\sqrt{\mathrm{i}}r)$ that satisfies Equation (11), in a square with a length of 2 for the following cases: (1) ψ is known on the boundary, and the solution is for $\partial\psi/\partial n$ on the boundary; (2) $\partial\psi/\partial n$ is known on the boundary, and the solution is for ψ on the boundary; and (3) ψ is known on two of the opposite sides but unknown on the rest of the boundary on which $\partial\psi/\partial n$ is known, and the solution is for $\partial\psi/\partial n$ on the two opposite sides and for ψ on the rest of the boundary. The three cases represent the so-called *Dirichlet* problem, *Neumann* problem and mixed problem respectively. The numerical solutions show very good accuracy.

For the fluid sloshing problem, there are four unknown complex functions on the boundary, i.e. ϕ, ψ, $\partial\phi/\partial n$ and $\partial\psi/\partial n$, and accordingly, there are four equations for their solutions, i.e. Equation (16), (20), (12) and (13) and/or Equation (14) and (15).

The terms $\partial\phi/\partial s$, $\partial\psi/\partial s$, $\partial^2\phi/\partial s^2$ and $\partial^2\psi/\partial s^2$ in the boundary conditions can be treated numerically without regarding them as independent unknown functions.

4. NUMERICAL PROCEDURE

Two-node linear boundary elements are used to discretize the boundary. The integral singularities are treated in the same way as in Reference [18]. The boundary conditions, Equations (12)–(15) are treated numerically by a five-point finite difference as

$$\left(\frac{\partial\phi}{\partial s}\right)_0 = \frac{1}{\sqrt{m}}\left(\frac{1}{12}\,\phi_{-2} - \frac{2}{3}\,\phi_{-1} + \frac{2}{3}\,\phi_1 - \frac{1}{12}\,\phi_2\right), \tag{21}$$

$$\left(\frac{\partial^2\phi}{\partial s^2}\right)_0 = \frac{1}{m^2}\left[-\frac{1}{12}(m+2n)\phi_{-2} + \frac{4}{3}(m+n)\phi_{-1} - \frac{5}{2}m\phi_0 + \frac{4}{3}(m-n)\phi_1 - \frac{1}{12}(m-2n)\phi_2\right], \tag{22}$$

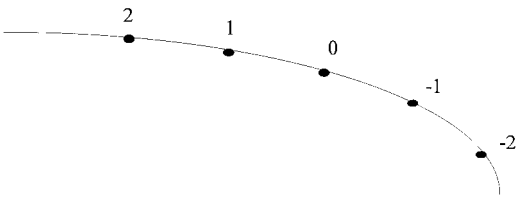

Figure 2. Five-point finite difference.

where

$$m = a_1^2 + b_1^2, \qquad n = a_1 a_2 + b_1 b_2,$$

$$a_1 = \frac{1}{12}x_{-2} - \frac{2}{3}x_{-1} + \frac{2}{3}x_1 - \frac{1}{12}x_2, \quad a_2 = -\frac{1}{24}x_{-2} + \frac{2}{3}x_{-1} - \frac{5}{4}x_0 + \frac{2}{3}x_1 - \frac{1}{24}x_2,$$

$$b_1 = \frac{1}{12}y_{-2} - \frac{2}{3}y_{-1} + \frac{2}{3}y_1 - \frac{1}{12}y_2, \quad b_2 = -\frac{1}{24}y_{-2} + \frac{2}{3}y_{-1} - \frac{5}{4}y_0 + \frac{2}{3}y_1 - \frac{1}{24}y_2,$$

and the subscript 0 denotes the nodal point at which the derivatives are taken, the subscripts -1, -2, 1 and 2 denote the nodal points adjacent to nodal point 0 (see Figure 2).

5. FLUID SLOSHING IN RESPONSE TO THE STRUCTURAL ARBITRARY AMPLITUDE MOTIONS

So as not to lose generality, for simplification we assume the structure is the container. In the frequency domain, the motion equations of the container can be expressed in matrix form as

$$(-\omega^2\mathbf{M} - \mathrm{i}\omega\mathbf{C} + \mathbf{K})\mathbf{X} = \mathbf{F}_S + \mathbf{F}_f, \tag{23}$$

where $\mathbf{M}$ is the mass matrix of the container, $\mathbf{C}$ and $\mathbf{K}$ respectively are the damping matrix and the rigidity matrix of the container due to certain restrictions, $\mathbf{F}_S$ is the exciting force vector exclusive of the fluid dynamic load, $\mathbf{F}_f$ is the integral force vector acting on the container by the fluid sloshing, and $\mathbf{X}$ is the complex motion amplitudes of the container.

For unit amplitude motion of the container in its three rigid body motion models, the container's motion amplitudes are denoted as X, Y, θ respectively, and the fluid sloshing can be described as

$$\phi = X\phi_1 + Y\phi_2 + \theta\phi_3, \tag{24}$$

$$\psi = X\psi_1 + Y\psi_2 + \theta\psi_3, \tag{25}$$

where (ϕ_1, ψ_1), $(\phi_2\, \psi_2)$ and (ϕ_3, ψ_3) are functions describing the fluid sloshing in response to the container's unit amplitude motions in the three rigid body motion models respectively. The resultant forces and moments acting on the container may be obtained by integration of the normal and shear stresses as

$$F_x = -\int_{S_2} (\sigma_n n_1 - \tau_{ns} n_2)\, \mathrm{d}S,$$

$$F_y = -\int_{S_2} (\sigma_n n_2 - \tau_{ns} n_1)\, \mathrm{d}S,$$

$$F_\theta = -\int_{S_2} \{\sigma_n[n_2(x - x_c) - n_1(y - y_c)] + \tau_{ns}[n_1(x - x_c) + n_2(y - y_c)]\}\, \mathrm{d}S.$$

Considering the stress–strain relationships and boundary conditions, through some deduction we have the forces and moment acting on the container by the sloshing fluid as follows:

$$\mathbf{F}_f = \begin{Bmatrix} F_x \\ F_y \\ F_\theta \end{Bmatrix} = \begin{bmatrix} A_1 & A_2 & A_3 \\ B_1 & B_2 & B_3 \\ C_1 & C_2 & C_3 \end{bmatrix} \begin{Bmatrix} X \\ Y \\ \theta \end{Bmatrix} = \mathbf{AX}, \tag{26}$$

where

$$A_1 = \mathrm{i}\omega\rho \int_{S_2} (n_1\phi_1 - n_2\psi_1)\, \mathrm{d}S,$$

$$A_2 = \mathrm{i}\omega\rho \int_{S_2} (n_1\phi_2 - n_2\psi_2)\, \mathrm{d}S,$$

$$A_3 = \mathrm{i}\omega\rho \int_{S_2} (n_1\phi_3 - n_2\psi_3)\, \mathrm{d}S - 2\mu\mathrm{i}\omega(x_1 - x_0),$$

$$B_1 = \mathrm{i}\omega\rho \int_{S_2} (n_2\phi_1 + n_1\psi_1)\, \mathrm{d}S,$$

$$B_2 = \mathrm{i}\omega\rho \int_{S_2} (n_2\phi_2 + n_1\psi_2)\, \mathrm{d}S,$$

$$B_3 = \mathrm{i}\omega\rho \int_{S_2} (n_2\phi_3 + n_1\psi_3)\, \mathrm{d}S - 2\mu\mathrm{i}\omega(y_1 - y_0),$$

$$C_1 = \mathrm{i}\omega\rho \int_{S_2} \{[n_2(x-x_c) - n_1(y-y_c)]\phi_1 + [n_1(x-x_c) + n_2(y-y_c)]\psi_1\}\, \mathrm{d}S,$$

$$C_2 = \mathrm{i}\omega\rho \int_{S_2} \{[n_2(x-x_c) - n_1(y-y_c)]\phi_2 + [n_1(x-x_c) + n_2(y-y_c)]\psi_2\}\, \mathrm{d}S,$$

$$C_3 = \mathrm{i}\omega\rho \int_{S_2} \{[n_2(x-x_c) - n_1(y-y_c)]\phi_3 + [n_1(x-x_c) + n_2(y-y_c)]\psi_3\}\, \mathrm{d}S - 2\mu\mathrm{i}\omega \int_{S_2} [(x-x_c)n_1 + (y-y_c)n_2]\, \mathrm{d}S.$$

Substitution of Equation (26) into Equation (23) affords

$$(-\omega^2\mathbf{M} - \mathrm{i}\omega\mathbf{C} + \mathbf{K})\mathbf{X} = \mathbf{F}_S + \mathbf{A}\mathbf{X}$$

or

$$(-\omega^2\mathbf{M} - \mathrm{i}\omega\mathbf{C} + \mathbf{K} - \mathbf{A})\mathbf{X} = \mathbf{F}_S. \tag{27}$$

Separation of the real part and the imaginary part of matrix $\mathbf{A}$ gives the added mass and the added damping matrices to the container

$$\mathbf{A} = \mathrm{Re}\,\mathbf{A} + \mathrm{i}\,\mathrm{Im}\,\mathbf{A} = \omega^2\left(\frac{1}{\omega^2}\,\mathrm{Re}\,\mathbf{A}\right) + \mathrm{i}\omega\left(\frac{1}{\omega}\,\mathrm{Im}\,\mathbf{A}\right) = \omega^2\mathbf{M}_a + \mathrm{i}\omega\mathbf{C}_a,$$

where obviously

$$\mathbf{M}_a = \frac{1}{\omega^2}\,\mathrm{Re}\,\mathbf{A}, \tag{28}$$

$$\mathbf{C}_a = \frac{1}{\omega}\,\mathrm{Im}\,\mathbf{A}. \tag{29}$$

$\mathbf{M}_a$ and $\mathbf{C}_a$ are the added mass and the added damping matrices respectively to the container due to fluid sloshing. Thus, if the added mass and the added damping matrices are known, the container's motion equations can be obtained by adding the added mass and the added damping matrices to its mass and damping matrices respectively. Finally, the motion equations of the container (23) become

$$[-\omega^2(\mathbf{M} + \mathbf{M}_a) - \mathrm{i}\omega(\mathbf{C} + \mathbf{C}_a) + \mathbf{K}]\mathbf{X} = \mathbf{F}_S. \tag{30}$$

6. NUMERICAL EXAMPLES

To make use of the experimental results taken from Reference [4], the rectangular tanker with length $L = 0.6095$, water depth $H = 0.06$ is considered first. The fluid viscosity is $\mu = 0.00094$ and the fluid density is $\rho = 1000$. The first asymmetrical resonant frequency may be calculated from the linear theory [17]

$$\omega_r = \sqrt{\frac{\pi g}{L} \tanh\left(\frac{\pi H}{L}\right)} = 3.893264007.$$

In the figures, the relative frequency is defined as

$$\Omega = \frac{\omega}{\omega_r}.$$

Figure 3 shows the comparison of the maximum surface elevations with horizontal sinusoidal excitation computed from the linear potential theory and from the analysis model considering the fluid viscosity. Owing to the fluid viscosity at or near the resonant zone, the fluid sloshing is heavily damped (see Figures 7 and 8), the wave elevation would not grow linearly with time [4], and a steady state is achieved. When far away from the resonant zone,

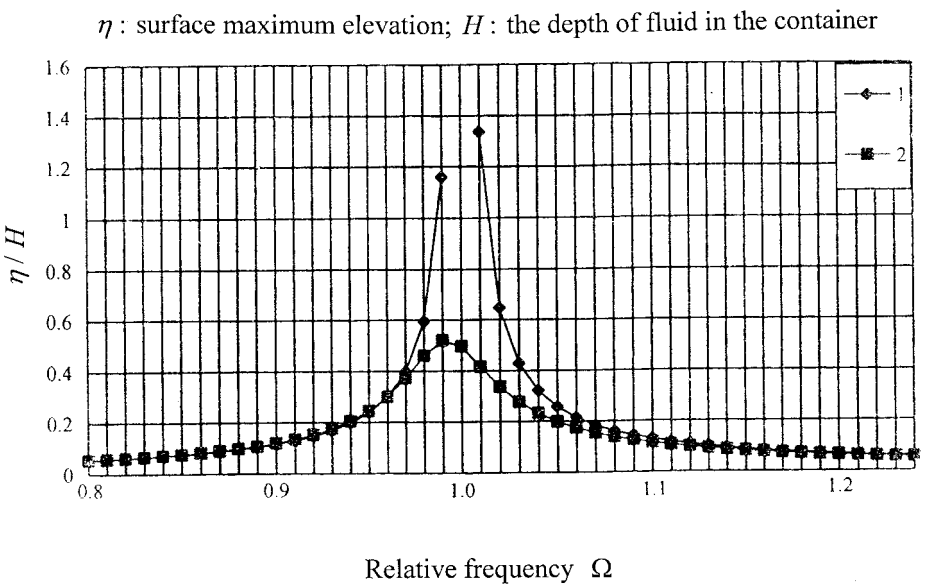

Figure 3. Surface wave elevation curves vs. the relative frequency (for horizontal excitation): curve 1, results of the linear potential theory; curve 2, results of the theory considering the fluid viscosity.

the results computed from the two theories almost coincide. Figures 4–6 show the added mass curves for m_{11}, m_{33} and m_{31}. The three figures of added mass curves have the same tendency that, across the resonant frequency, the values of the added mass for m_{11}, m_{33} and m_{31} change signs, which concurs with Reference[19]. The sign flips in Figures 3–6 are due to the too large values computed from the linear potential theory. It is impossible to show these data in the figures.

Figures 7–9 show the added damping curves for c_{11}, c_{33} and c_{31} respectively. The values of the added damping reach their maximum at the resonant frequency.

For the motion model in the vertical direction, the present model cannot describe the uneven surface motion [5]. The corresponding added damping c_{21}, c_{12}, c_{32}, c_{23} are all zero, since the fluid does not have relative motions to the container in this motion model. Thus, the added mass m_{22} should be the fluid mass in the container.

The convergence of the computations with nodal points is shown in Figure 10. Since for each nodal point, there are four complex unknowns, the total unknowns on the boundary amount to four times of the number of the boundary nodal points. The computer efforts are mainly put to the solutions of the simultaneous linear equations.

The comparison of the maximum wave elevation computed by the present model with that of the linear theory of [4] is shown in Figure 11.

The comparisons of the maximum wave elevation computed by the present model with that of the experiment taken from [4] are shown in Figure 12. At or near the resonant zone, the present model gives much better predictions than the linear potential theory, and for those frequencies away from the resonance ($\Omega < 0.94$ and $\Omega > 1.07$), the numerical results agree well with the experimental data.

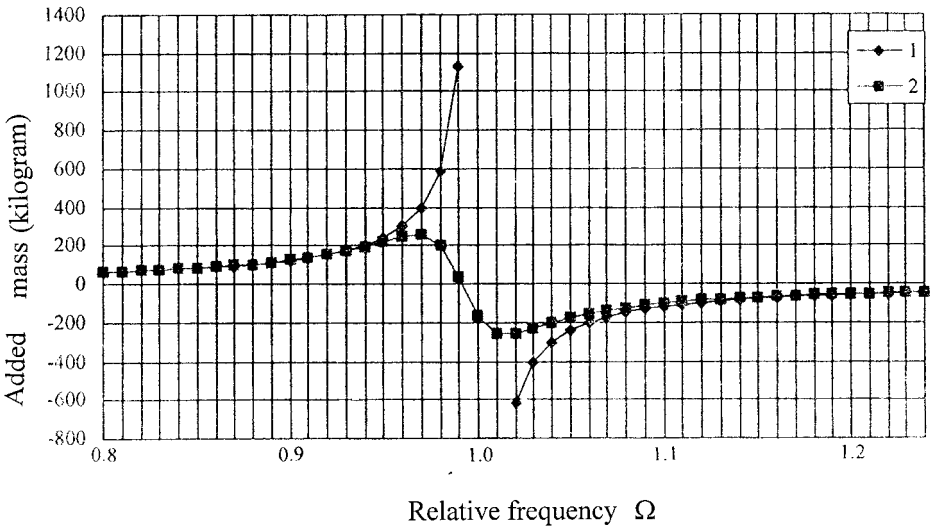

Figure 4. Added mass curves for m_{11} vs. the relative frequency: curve 1, results of the linear potential theory; curve 2, results of the theory considering the fluid viscosity.

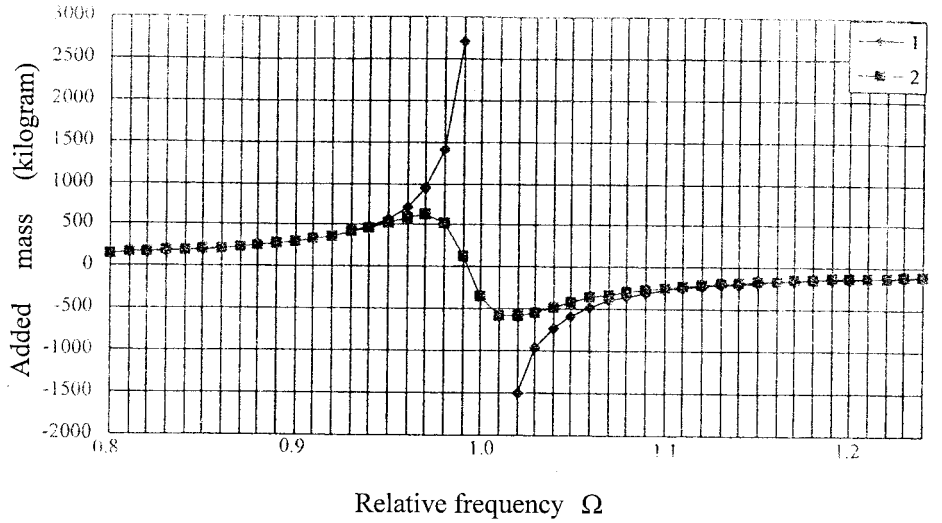

Figure 5. Added mass curves for m_{33} vs. the relative frequency: curve 1, results of the linear potential theory; curve 2, results of the theory considering the fluid viscosity.

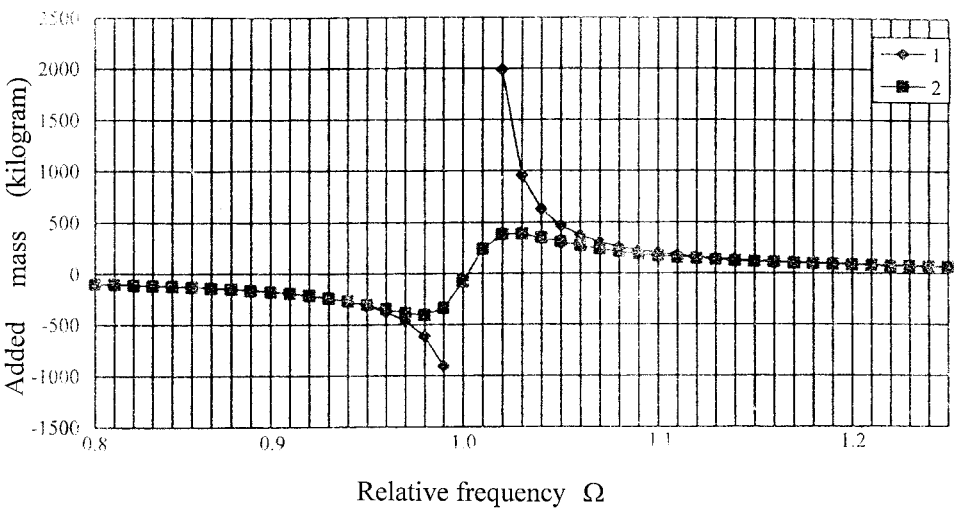

Figure 6. Added mass curves for m_{31} vs. the relative frequency: curve 1, results of the linear potential theory; curve 2, results of the theory considering the fluid viscosity.

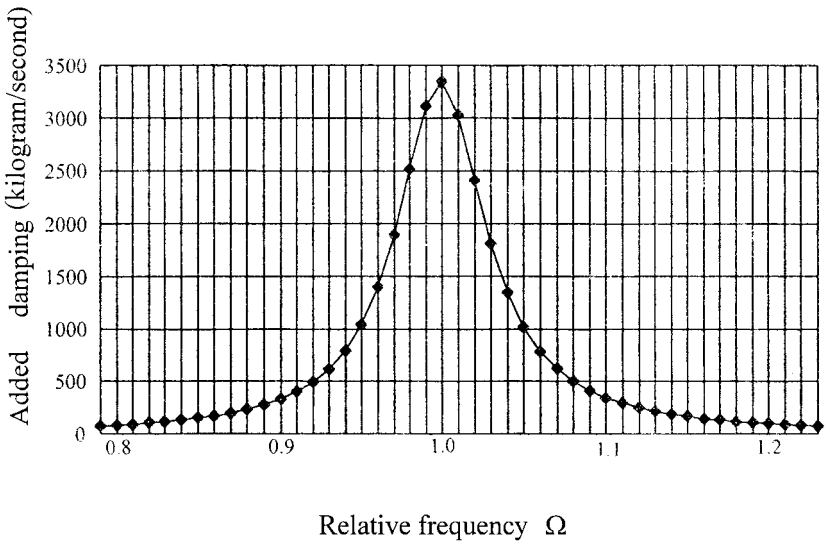

Figure 7. Added damping curve for c_{11} vs. the relative frequency.

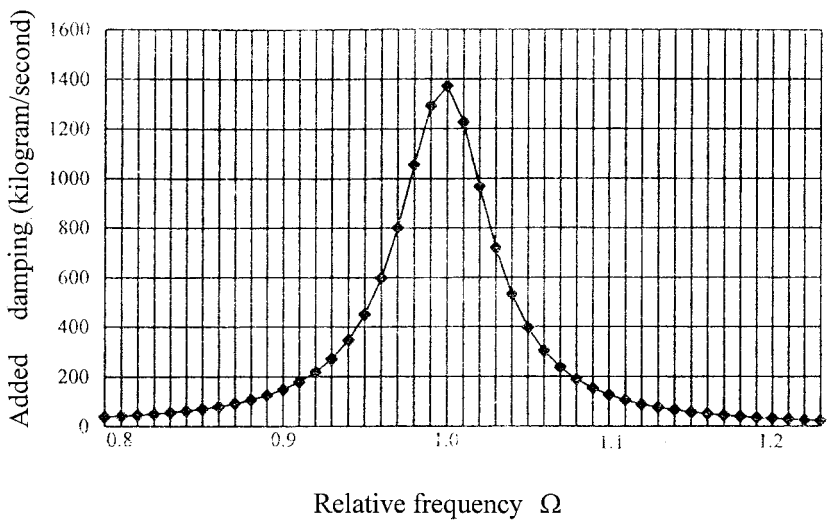

Figure 8. Added damping curve for c_{33} vs. the relative frequency.

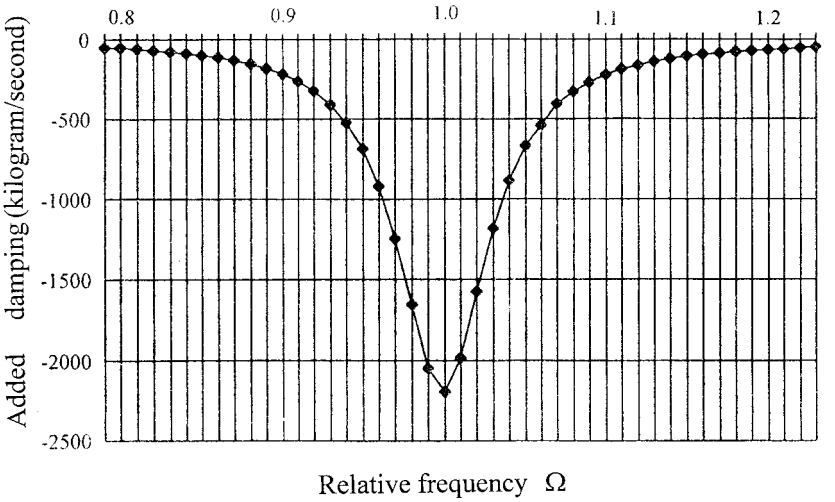

Figure 9. Added damping curve for c_{31} vs. the relative frequency.

Figure 13 shows the computed maximum wave elevations for different fluid viscosities with the same water depth, container size and the same excitation. From Figure 13, we can see that among the fluids, the fluid with viscosity $\mu = 0.00376$ gives the highest surface elevation, and with the increase of the viscosity, the resonant frequency of the fluid becomes smaller.

Computations are also carried out for the example used in [13] for the verification of pitch motions. It is, again, a rectangular tank with length $L = 0.59$ and water depth $H = 0.04$. The fluid viscosity is taken to be $\mu = 0.00105$, and the excitation angle is taken to be $\theta = 0.1°$. The resonant frequency of the linear potential theory is

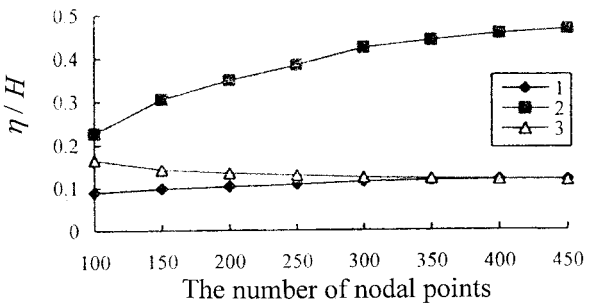

Figure 10. Convergence of the maximum wave elevation with nodal points. Curve 1, maximum elevation for $\omega = 3.698601$ ($\Omega = 0.95$); curve 2, maximum elevation for $\omega = 3.893264$ ($\Omega = 1.00$); curve 3, maximum elevation for $\omega = 4.087927$ ($\Omega = 1.05$); η, surface maximum elevation; H, the depth of fluid in the container.

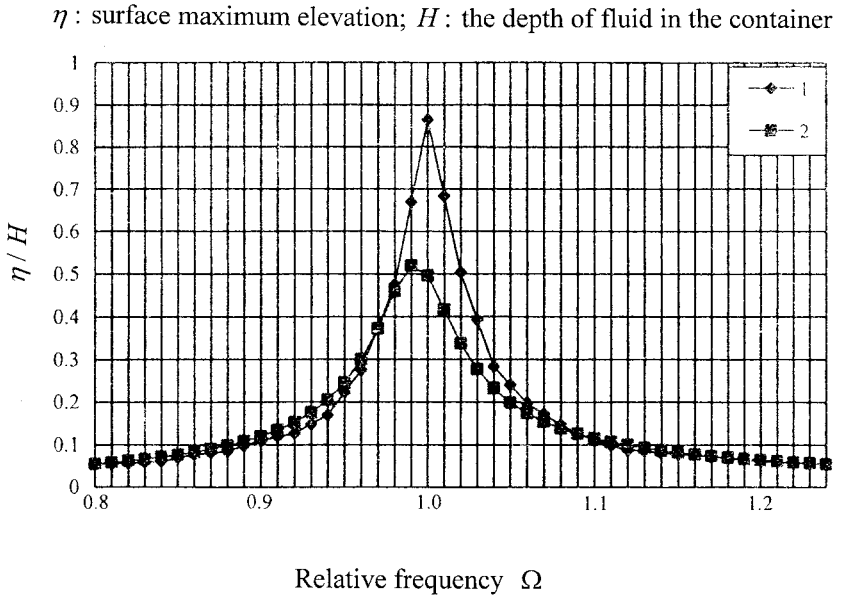

Figure 11. Comparison of maximum wave elevation with the linear theory of [4]. Curve 1, results of the linear theory of [4]; curve 2, results of the theory considering the fluid viscosity of the present theory; η, surface maximum elevation; H, the depth of fluid in the container.

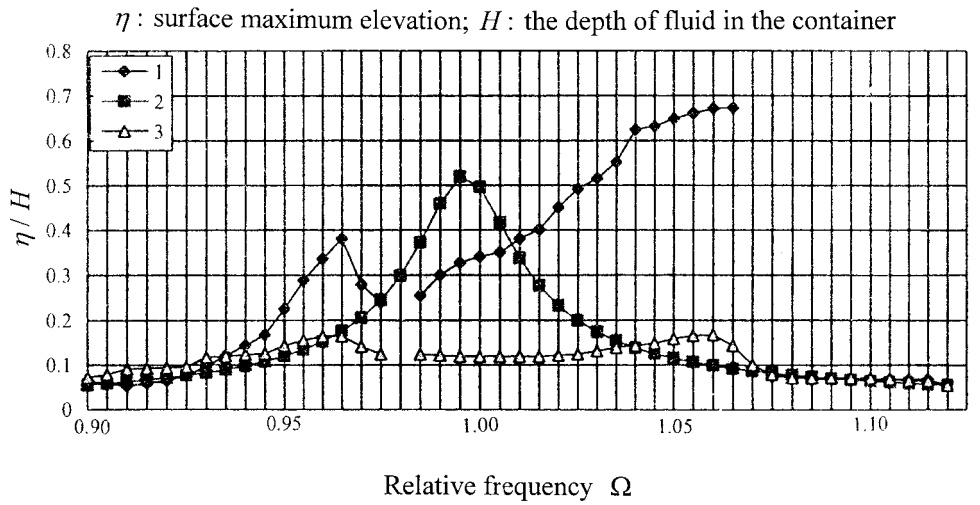

Figure 12. Comparison of maximum wave elevation with the experiment in [4]. Curve 1, results of the experiment for peak elevations; curve 2, results of the present paper; curve 3, results of the experiment for trough elevations.

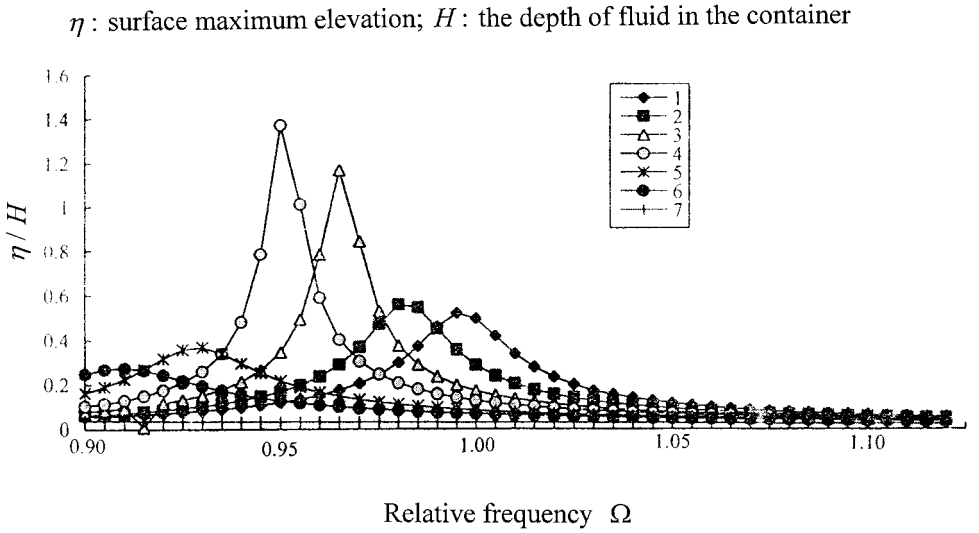

Figure 13. Maximum elevations for fluid with different viscosities. Curve 1, results for fluid of viscosity $\mu = 0.00094$; curve 2, results for fluid of viscosity $\mu = 0.00188$; curve 3, results for fluid of viscosity $\mu = 0.00282$; curve 4, results for fluid of viscosity $\mu = 0.00376$; curve 5, results for fluid of viscosity $\mu = 0.00470$; curve 6, results for fluid of viscosity $\mu = 0.00564$; curve 7, results for fluid of viscosity $\mu = 0.00940$.

$$\omega_r = \sqrt{\frac{\pi g}{L} \tanh\left(\frac{\pi H}{L}\right)} = 3.310648639.$$

The comparison of the surface elevation is shown in Figure 14. The positive wave elevation (peak) curve fits well to the experimental data taken from [13]. For the present model, owing to the linearization of the free surface condition, the negative wave elevation (trough) is equal to the positive elevation. However, the experimental data show that the negative wave elevation is not equal to the positive elevation at or near the resonant zone. Obviously, this is caused by the non-linearity of the free surface condition.

7. CONCLUSIONS

A BEM is presented for the coupled motion analysis of fluid sloshing and structural vibrations. In the present model, the fluid viscosity is considered, and the non-slip boundary conditions are imposed on the interface of the fluid and the container's walls. A coupled motion analysis is carried out for the container with fluid and this method can be extended to the coupled motion analysis of an arbitrary structure on which a container with fluid is mounted.

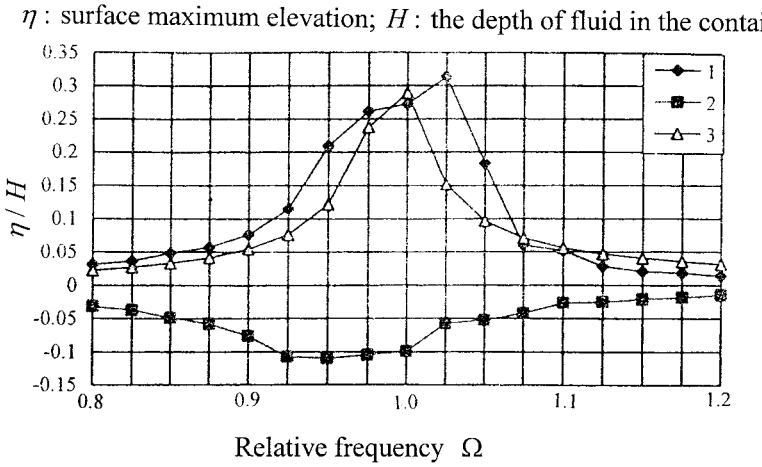

Figure 14. Comparison of the maximum wave elevation for pitch motion. Curve 1, results of the experiment of [13] for peak elevation; curve 2, results of the experiment of [13] for trough elevation; curve 3, results of the present paper considering the fluid viscosity.

REFERENCES

1. M. Ikegawa, 'Finite element analysis of fluid motion in a container', in J.T. Oden, O.C. Zienkiewicz, R.H. Gallagher and C. Taylor (eds.), *Finite Element Methods in Flow Problems*, UAH Press, Huntsville, 1974, pp. 737–738.
2. K. Washizu, T. Nakayama and M. Ikegawa, 'Application of the finite element method to some free surface fluid problems', in W.G. Gray, G.F. Pinder and C.A. Brebbia, *Finite Elements in Water Resources*, Pentech Press, London, 1978, pp. 4.247–4.266.
3. T. Nakayama and K. Washizu, 'Nonlinear analysis of liquid motion in a container subjected to forced pitching oscillation', *Int. J. Numer. Methods Eng.*, **15**, 1207–1220 (1980).
4. T.G. Lepelletier and F. Raichlen, 'Nonlinear oscillations in rectangular tanks', *J. Eng. Mech.*, **114**, 1–23 (1988).
5. T. Nakayama and K. Washizu, 'The boundary element method applied to the analysis of two-dimensional nonlinear sloshing problems', *Int. J. Numer. Methods Eng.*, **17**, 1631–1646 (1981).
6. T. Nakayama, 'Boundary element analysis of nonlinear water wave problems', *Int. J. Numer. Methods Eng.*, **19**, 953 (1983).
7. N. Tosaka and R. Sugino, 'Boundary element analysis of potential flow with nonlinear free surface', *Proc. 4th China–Japan Symp. on Boundary Element Methods*, 1991, pp. 137–144.
8. A. Shinkai, K. Yamaguchi and J. Fukuda, 'Numerical analysis of three-dimensional sloshing problem', *Trans. West-Japan Society of Naval Architects*, No. 64, 1982, pp. 103–117.
9. A. Shinkai, K. Yamaguchi and J. Fukuda, 'Numerical analysis of three-dimensional sloshing problem (continued)', *Trans. West-Japan Society of Naval Architects*, No. 66, 1983, pp. 25–35.
10. T. Ohyama and K. Fujii, 'A boundary element method analysis for two-dimensional nonlinear sloshing problem', *JSCE J. Struct. Eng.*, **35A**, 575–584 (1989) (in Japanese).
11. L.M. Sun, Y. Fujino, B.M. Pacheco and M. Isabe, 'Nonlinear waves and dynamic pressures in rectangular TLD-simulation and experimental verification', *J. Struct. Eng. Earthquake Eng., Proc. JSCE*, **6**, 251–262 (1989).
12. Y. Fujino, L.M. Sun, B.M. Pacheco and P. Chaiseri, 'Tuned liquid damper for suppressing horizontal motion of structures', *ASCE J. Eng. Mech.*, **118**, 2017–2030 (1992).
13. L.M. Sun, Y. Fujino and K. Koga, 'A model of tuned liquid damper (TLD) for suppressing pitching motions of structure', *Earthquake Eng. Struct. Dyn.*, **24**, 625–636 (1995).
14. L.M. Sun and Y. Fujino, 'A semi-analytical model for tuned liquid damper (TLD) with wave breaking', *J. Fluids Struct.*, **8**, 471–488 (1994).

15. Y. Fujino and L.M. Sun, 'Vibration control by multiple tuned liquid dampers (MTLDS)', *ASCE J. Struct. Eng.*, **119**, 3484–3502 (1993).
16. V.J. Modi and F. Welt, 'Vibration control using nutation dampers', *Proc. Int. Conf. on Flow Induced Vibrations*, BHRA, UK, 1987, pp. 369–376.
17. H. Lamb, *Hydrodynamics*, 6th edn., Cambridge University Press, Cambridge, 1932, pp. 619–621.
18. Y. Zang and X. Ji, 'A scheme of eliminating integral singularity in boundary element method', *Acta Mech. Solida Sinica*, **15**, 161–165 (1994).
19. L.M. Sun, Y. Fujino, P. Chaiseri and B.M. Pacheco, 'The properties of tuned liquid dampers using a TMD analogy', *Earthquake Eng. Dyn.*, **24**, 967–976 (1995).
20. G.N. Watson, *A Treatise on the Theory of Bessel Functions*, Cambridge University Press, Cambridge, 1944.

